Localization and steric effect of the lone electron pair of the tellurium Te 4+ cation and other cations of the p -block elements. A systematic study

David Hamani, Olivier Masson, Philippe Thomas

Localization and steric effect of the lone electron pair of tellurium Te^{4+} cation and other cations of the p-block elements. A systematic study.

D. Hamani, O. Masson *, P. Thomas

Institut de Recherche sur les Céramiques (IRCER) – UMR CNRS 7315, Université de Limoges, Centre Européen de la Céramique, 12 rue Atlantis, 87068 Limoges Cedex, France.

* Corresponding author: Olivier Masson, E-mail: olivier.masson@unilim.fr

Keywords

Lone electron pair; localization; steric effect; geometrical method; tellurium(IV) oxide.

Abstract

We developed a simple method based on pure geometrical concepts to localize lone pairs (LP) of cations of the p-block elements and model their steric effect. The method was applied to 1185 structures containing LP cations in 2439 non-equivalent positions. For oxide crystal structures, it is observed that going from bottom left to top right in the periodic table, LP moves away from the cation core and decreases in size. For a given kind of cation M*, the LP radius increases linearly with the M*-LP distance, the smallest rate being observed for Tl^{+} and the largest for Cl^{5+}. The influence of the anion type was also studied in the case of the Te^{4+} cation. Overall, the same trends are observed. The smallest Te-LP distances and LP radii are found for anions of large size and small charge.

1. Introduction

Cations of the p-block elements (M*), when bonded to anions such as O^{2-}, F^-, Cl^-, may present a lone electron pair (LP) with stereochemical activity responsible for asymmetric atomic environments. This phenomenon, usually explained with the valence shell electron pair repulsion (VSEPR) theory of Gillespie & Nyholm (1957), can play a significant role on the properties of many compounds. As an example, the remarkable nonlinear optical properties of tellurite (*i.e.* TeO_2-based) materials are known to be partly due to the activity of the $5s^2$ lone electron pair of Te^{4+} cations (Fargin *et al.*, 1996; Jeansannetas *et al.*, 1999; Suehara *et al.*, 2004*b*,*a*; Soulis *et al.*, 2008; Roginskii *et al.*, 2017). The position and steric effect of LP are thus valuable parameters for understanding the structure-properties relationships of some inorganic compounds and must be assessed by experimental or theoretical methods.

The volume occupied by lone pairs in crystalline compounds was first estimated experimentally by Andersson & Åström (1972) who noticed that the average available volume for anions is larger in compounds with LP cations than without. Thanks to the difference between these volumes, they estimated that the lone pairs occupy an effective volume similar to that of the anions. Experimental localization of LP of cations appears later through the study of electronic density maps obtained by X-ray diffraction methods (Kondratyuk *et al.* (1987) for α-TeO_2 crystal). This kind of analysis, while interesting, is generally complex to implement and not suited for systematic studies. In this context, modeling is an invaluable tool, but to date only few methods exist to localize LPs or estimate their steric effect.

The first modeling method was introduced by Galy *et al.* (1975). It was based on geometrical concepts considering that LP cations are located in the center of a regular polyhedron

(tetrahedron, triangular bipyramid or octahedron) made of LP and surrounding anions. The

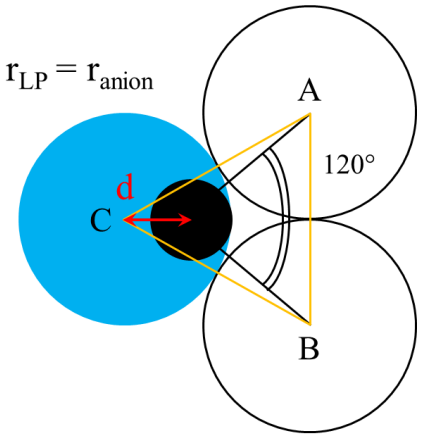

principle of the method, illustrated in Figure 1, entails that LPs and anions are modeled by spheres of equal size. In this pioneering work, Galy *et al.* systematically calculated the M*-LP distances found in 48 non-equivalent environments of 40 crystal structures containing 12 LP cation types and determined trends relating the average M*-LP distances to the position of the elements in the periodic table. While powerful, this method assumes a regular polyhedron around the LP cation and works poorly with structures with not compact enough anionic packing, *e.g.* with heavy LP cations such as Tl^{+}, Pb^{2+} and Bi^{3+}. More recently, another geometrical method using the algorithm initially proposed by Balić Žunić & Makovicky (1996) was applied to determine the LP stereoactivity in TeO_2-based structures (Christy & Mills, 2013). The stereoactivity was estimated as the distance between the Te^{4+} core and the center of a large sphere as close as possible to the centers of the neighboring anions. A linear correlation was found by the authors between this distance and the radius of the sphere, highlighting the fact that the lone pair repels the neighboring anions.

In 1978, Verbaere *et al.* (1978) proposed a non-geometrical method based on the calculation of the local electric field around LP cations in order to obtain the cation polarization. This method requires the knowledge of both the charges and polarizabilities of all the ions in the system. It was first applied on crystal structures containing Tl^{+} cations and was later on implemented in the HYBRIDE program (Wallez, 1999).

More recently, quantum chemistry calculations using the electron localization function (ELF) introduced by Becke & Edgecombe (1990) was used to visualize and analyze lone pairs in different compounds (*e.g.* Chesnut, 2000; Seshadri, 2001; Berski *et al.*, 2007; Rahm & Christe, 2013). Based on the Pauli Exclusion Principle, ELF associates a value to every point in space depending on the probability of finding two electrons with same spin. ELF maps can be used to localize lone pairs by identifying high ELF values in the LP cation neighborhood. The ELF method has been applied for instance in the case of compounds containing Te^{4+} (Hamani, 2010), Tl^{+} to Po^{4+} (Matar & Galy, 2015; Galy & Matar, 2016), N^{3+} to Bi^{3+} cations (Galy *et al.*, 2017; Galy & Matar, 2018; Galy & Vignoles, 2020) and Sn^{2+} (Galy & Matar, 2019). This procedure is however highly demanding and requires generally long-time computer calculations.

In this paper, we present a new and simple method able to localize lone pairs and determine their steric effect in various chemical systems. It is based on pure geometrical concepts and requires no *a priori* knowledge apart from the ionic radii. The description of the method is presented in § 2. Its application and the analysis of the evolutions of the M*-LP distance and LP radius as functions of the cation type is presented in § 3 using 1138 oxide crystal structures containing As^{3+}, Bi^{3+}, Br^{5+}, Cl^{5+}, Ga^{+}, Ge^{2+}, I^{5+}, In^{+}, P^{3+}, Pb^{2+}, S^{4+}, Sb^{3+}, Se^{4+}, Sn^{2+}, Te^{4+}, Tl^{+} or Xe^{6+} cations in 2380 non-equivalent positions. In § 4, emphasis is given to TeO_2-based structures and to the influence of the anion type (X) within 47 non-oxide Te_mX_n-based structures containing 59 non-equivalent Te^{4+} positions.

2. The lone pair localization method

The principle of the method is based on the fact that space can be filled with hard spheres representing anions, LP cation cores and LPs, each LP cation being decomposed into a core and a lone pair. LP cations have asymmetric environments characterized by a neighboring empty space (*i.e.* not occupied by anions) which can partly be filled with a sphere modeling

the steric effect of the lone pair. The positions and radii of anions and LP cation cores are fixed whereas the position and radius of LP are adjusted to best fill the empty space. To our knowledge, such a problem has no analytical solution and must be solved numerically. We used the following procedure. The position and radius of the lone pair are varied in order to minimize the sum of distances (SoD) between LP and the neighboring anion surfaces (*i.e.* the length of empty space between LP and anions), calculated as follows:

$$SoD = \sum_{k} (d_{LP-k} - r_{LP} - r_k)$$

where d_{LP-k} is the distance between the centers of the lone pair and a neighboring anion k, r_{LP} is the LP radius and r_k is the radius of anion k. The sum is performed over all anions which lie within a given cut-off distance from the LP cation core. All the terms in SoD are positive or null, *i.e.* no interpenetration between the LP sphere and the neighboring spheres is allowed. The retained LP position and size values are those which minimize SoD. In practice, a spherical coordinate system is used to sample the unit-cell volume using constant angular and radial steps. A constant step is also used to sample r_{LP}. The procedure is illustrated in

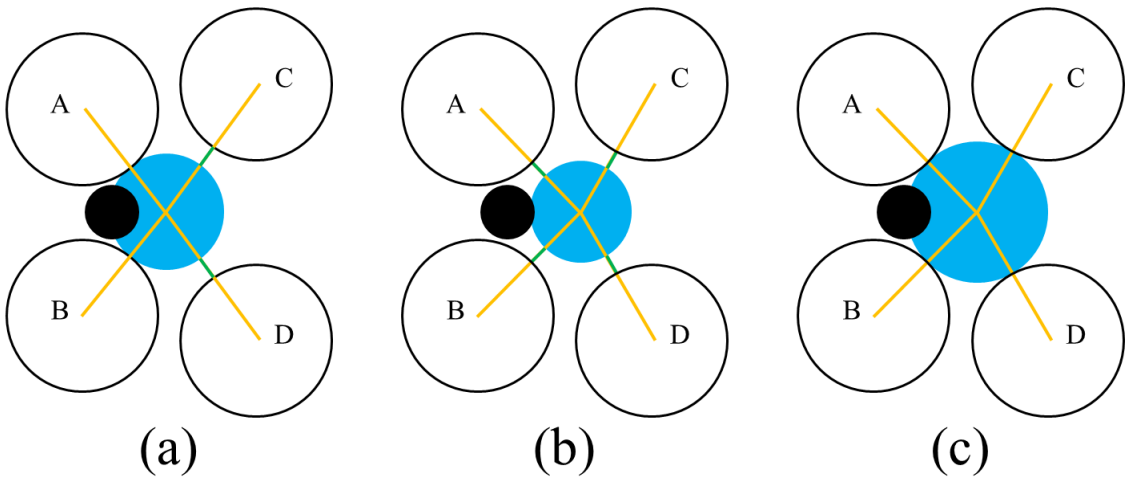

Figure 2. Typical results are illustrated by

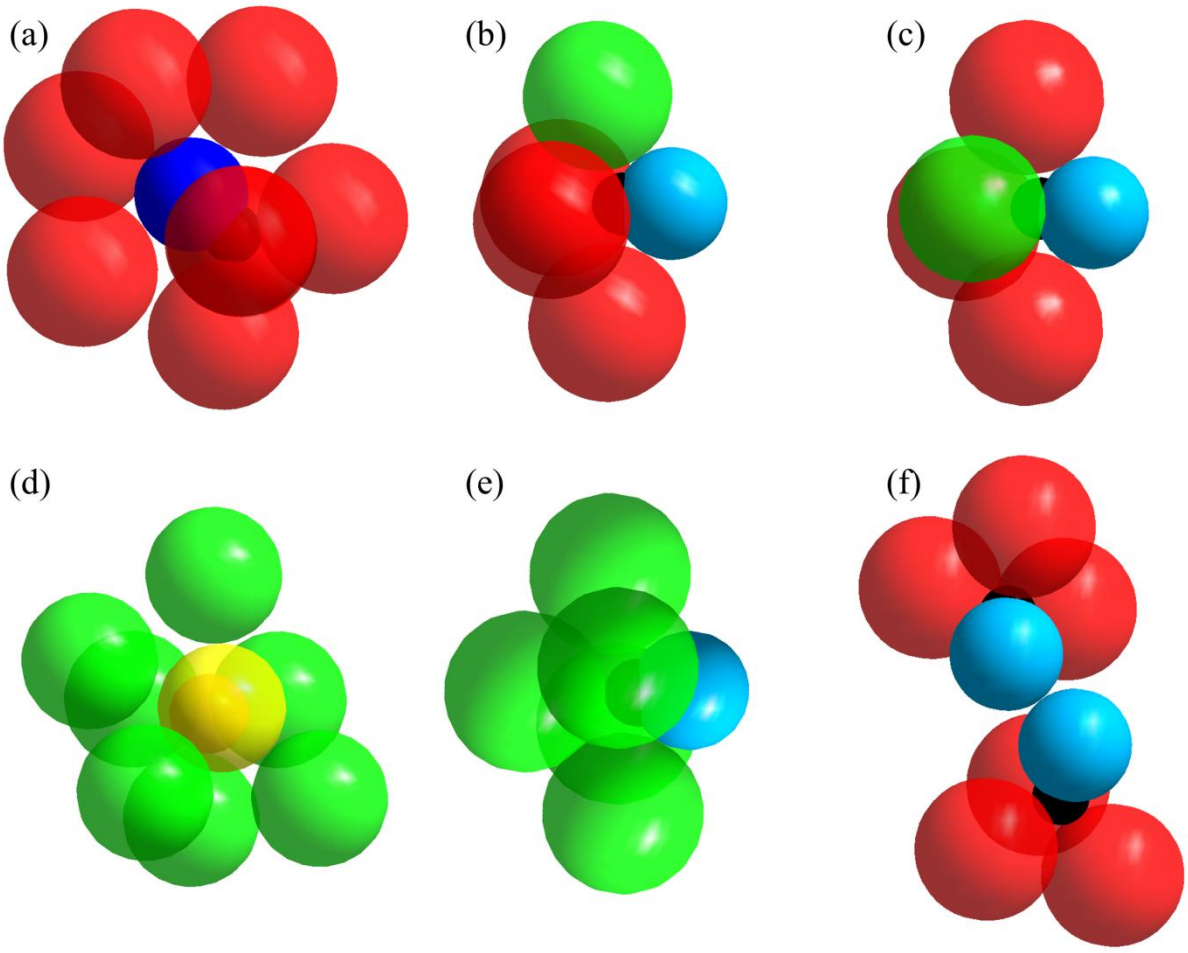

Figure 3 (a, b, c, d and e) for the cases of α-TeO_2 (a), $Te_2O_3F_2$ (b, c) which contains two anion types and $PbTeF_6$ (d, e) which contains two LP cation types.

In the case of more open structures, the procedure must be refined in two ways in order to avoid unrealistic large displacement of a lone pair with respect to its core. First, the LP displacement is limited so as to maintain contact with the core. This condition is satisfied by verifying that the M*-LP distance is lower than or equal to the sum of radii of the lone pair and its cation core. In practice, considering that the lone pair has a negative charge of -2, an efficient choice for the radius of the cation core is to take the ionic radius of the cation with a charge number augmented by +2 (*e.g.* ionic radius of Te^{6+} for the Te^{4+} core). Second, as in

some structures the lone pairs face each other, the SoD criterion is modified such as to avoid interpenetration between facing lone pairs, as follows:

$$SoD = \sum_i \left(\sum_k (d_{LPi-k} - r_{LP} - r_k) + \sum_{j\,(i \neq j)} (d_{LPi-LPj} - 2 * r_{LP}) \right)$$

where $d_{LPi-LPj}$ is the distance between lone pairs LP_i and LP_j, the sum over i being taken for all lone pairs facing each other. In order to have a unique solution, all facing LPs are considered to have the same radius. This is exact when facing LPs belong to cations of equivalent positions. In most other cases the induced error is expected to be small, in particular when the lone pairs belong to cations with close positions in the periodic table. The results of the procedure in the case of facing LPs are illustrated in

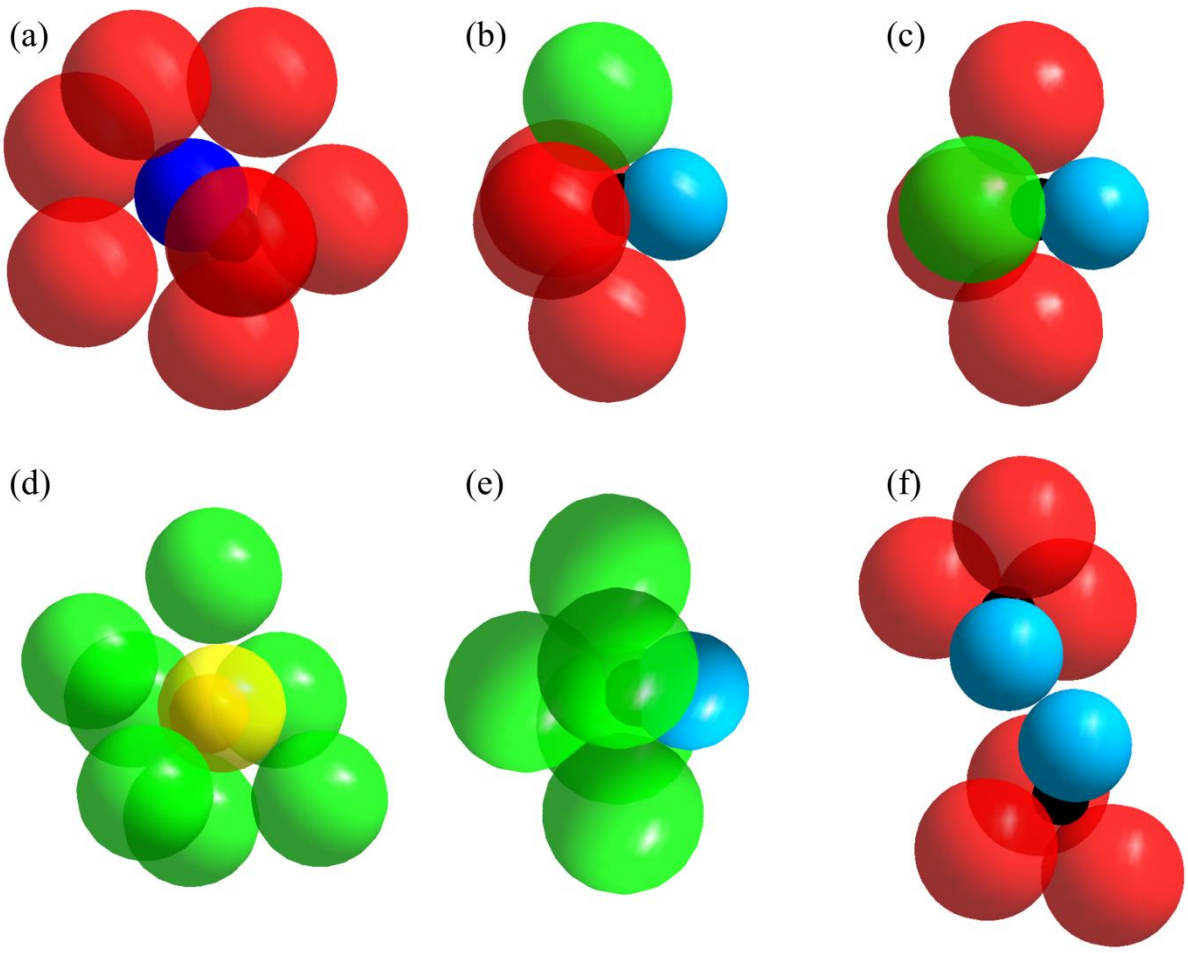

Figure 3 (f) for α-$CdTeO_3$ where the lone pairs of Te^{4+} ions from two non-equivalent positions face each other.

The presented procedure requires the choice of a cut-off radius as well as ionic radii. The effect of these parameters on the results was tested as follows. Regarding the cut-off radius, it appeared that the average M*-LP distance and LP radius converge to stable values for a cut-off larger than 6 Å (see supporting information S1). In practice, a cut-off of 10 Å is a good choice as it ensures converged values in all cases without impacting too much the computation time. Regarding the choice of the ionic radii, both crystal radii and effective radii (Shannon, 1976) were tested. The effect on M*-LP distance is small. Over 2439 non-equivalent LP cation positions, the average M*-LP distance was 0.83 Å using crystal radii versus 0.86 Å using effective radii, *i.e.* a relative variation of less than 4%. The localization method is thus mostly insensitive to the choice of ionic radii. The LP radius is however more affected by ionic radii. The average LP radius was 1.27 Å using crystal radii versus 1.15 Å using effective radii, *i.e.* a relative variation of more than 10 %. This effect can be explained by the fact that smaller anion radii (crystal radii) free more space around the LP cation cores and thus induce larger LP radii. Whatever the chosen radii, the relative evolutions of the M*-LP distance and LP radius as functions of M* did not change.

The method was implemented in a program written in C++ language, 'LPLoc' (Hamani & Masson, 2019). The input is a Crystallographic Information File (CIF) (Hall *et al.*, 1991; (*a*)) containing at least the space group with the lattice parameters and the atomic positions of the analyzed structure. The user can choose the cut-off radius and select either crystal or effective ionic radii or input his/her own radius values. Calculations took a few seconds to a few dozen seconds, depending on the complexity of the structure, on a personal computer with Intel® Core™ i5-2500K CPU @ 3.30 GHz and 4.00 Go RAM.

3. Results and discussion

All the results presented in this section were obtained using effective ionic radii and a cut-off radius of 10 Å. The CIF files of the analyzed structures were extracted from the Inorganic Chemistry Structure Database (ICSD) (*b*). The structure selection criteria and the full results are listed in supporting information S2.

3.1. Evolutions of the M*-LP distances and LP radii within the periodic table for cations of p-block elements in oxide crystal structures

The method was applied to 1138 oxide crystal structures containing LP cations of p-block elements in order to establish trends in the evolutions of M*-LP distances and LP radii within the periodic table. This corresponds to 2380 non-equivalent positions of As^{3+}, Bi^{3+}, Br^{5+}, Cl^{5+}, Ga^{+}, Ge^{2+}, I^{5+}, In^{+}, P^{3+}, Pb^{2+}, S^{4+}, Sb^{3+}, Se^{4+}, Sn^{2+}, Te^{4+}, Tl^{+} and Xe^{6+}.

The average M*-LP distances and LP radii are reported in Table 1 and are represented schematically in Figure 4 according to the positions of the elements in the periodic table. We note that the M*-LP distances tend to decrease down a group, with the exceptions of Ga^{+} and In^{+}, for which only one structure was valuable from the database, and of the very small S^{4+} and Cl^{5+} cations. The trend along a period is less clear. Things are different if we instead consider the relative displacement (RD) of the lone pair away from its core with respect to the cation core and LP sizes, using the relation

$$RD = d_{M^*\text{-}LP}/(r_{M^*}+r_{LP}),$$

where $d_{M^*\text{-}LP}$, r_{M^*} and r_{LP} are the average M*-LP distance, the core radius and the average LP radius respectively. This permits taking into account the size effect of the cation. The relative displacement can vary between 0% (*i.e.* LP is not active stereochemically) and 100% (*i.e.* the core is completely naked, the lone pair being tangent to the core). The obtained RD values are reported in Table 1 and Figure 4. Minimal relative displacements are found at the bottom left for Tl^{+} (13%), In^{+} (3%) and Ga^{+} (0%) and maximal ones at the top right for S^{4+} and Cl^{5+} (93% for both). We now observe clear trends: the relative displacements decrease down a group and

increase from left to right in a period. This results confirm the previous works (Galy *et al.*, 1975) and generalize them to a large number of compounds.

The decrease of the relative M*-LP distance down a group means that for a given cation charge, the smaller the core radius, the larger the M*-LP distance. This evolution can be related to the bond valence distortion theorem (Allmann, 1975; Brown, 1978; Urusov, 2003; Brown, 2011, 2016). A large LP displacement allows the anions located at the opposite side of the lone pair to get closer to the core, which in turn allows the formation of cation-anion bonds with large bond valences, *i.e.* primary bonds. Thus for cation with small core size, a large LP displacement enables the cation to reach its ideal valence (*i.e.* its formal charge) with only primary bonds. On the contrary, in the case of large core radius, the cation valence cannot be satisfied anymore with primary bonds. A small LP displacement is thus mandatory to increase the number of secondary bonds which supply the missing bond valences.

The increase of the relative M*-LP distance observed from left to right in a period (*i.e.* from less charged to more charged cations) can also be explained with the bond valence distortion theorem. Indeed, a highly charged cation, *i.e.* with small core radius, must undergo a large LP displacement in order to favor shorter cation-anion distances and reach its high valence.

Similarly, when the lone pair sufficiently displaces away from the core, it also partially bares the latter. The relative volume (RV) of the naked part of the core with respect to the full core volume, $RV = V_{naked\_M*}/V_{M*}$ (where V_{naked_M*} and V_{M*} are the volumes of the naked part and the core respectively), is reported in Table 1 and Figure 4 for each LP cation type. This parameter is related to RD and thus has a similar evolution within the periodic table. A zero relative volume is observed at the bottom left for Ga^{+}, In^{+}, Tl^{+} and Pb^{2+} and the largest values are obtained at the top right for S^{4+} (98%) and Cl^{5+} (99%). The cores of Ga^{+}, In^{+}, Tl^{+} and Pb^{2+} are thus fully enclosed within the lone pair while the cores of S^{4+} and Cl^{5+} are almost totally naked.

Regarding the average LP radii (Table 1 and Figure 4) and except for the very small S^{4+} and Cl^{5+} cations of the third period, we found little variation in a group (1.46 Å in average for M^{+}, 1.33 Å for M^{2+}, 1.16 Å for M^{3+}, 1.08 Å for M^{4+}, 0.99 Å for M^{5+} and 0.84 Å for M^{6+}). We did not observe an overall increase down a group, as we could have expected from the general trends of the ionic radii. From left to right however, the LP radii clearly decrease, suggesting that they are mainly related to the cation charge.

The evolutions of the LP radius as a function of the M*-LP distance for the different elements are plotted in Figure 5. There is a clear positive and linear correlation between these two parameters, indicating that the longer the M*-LP distance, the larger the LP radius. The variations are more or less pronounced depending on the element. Overall, the slope increases from bottom left to top right, with a value of 0.10 for Tl^{+} (*i.e.* the LP radius is almost insensitive to the M*-LP distance) and 0.96 for Cl^{5+}. Clearly, the higher the slope, the smaller the cation radius. The intercept at the origin can be thought as the cation radius when the LP is stereochemically inactive.

3.2. The specific case of the Te^{4+} cation

3.2.1. Oxide crystal structures

This part focuses on TeO_2-based structures, for which the presence of LP on Te^{4+} cations induces asymmetric environments and large variations of the coordination number depending on the type and quantity of added modifier oxides. A recent review of the structural features of these compounds is given by Christy *et al.* (2016).

In the reference structure α-TeO_2, all Te^{4+} cations are four-fold coordinated and form TeO_4 disphenoids presenting two short equatorial bonds (Te-O_{eq} = 1.88 Å) and two longer axial bonds (Te-O_{ax} = 2.12 Å) (Kondratyuk *et al.*, 1987). When adding modifier oxides, the TeO_4 units transform into TeO_{3+1} (deformed disphenoids with one lengthened bond) and TeO_3 units (triangular pyramids) in varied proportions (Figure 6) (*e.g.* Tagg *et al.*, 1994; Becker *et al.*,

1997; Mirgorodsky *et al.*, 2002). Besides these three usual environments, atypical environments are also described in the literature, such as five-fold coordination (for instance in $BaTe_2O_6$, $K_2Te_4O_{12}$, $NiTe_2O_5$, $SrTe_3O_8$ and $P_2Te_3O_{11}$) and a very rare six-fold coordination reported in $Cs_2Te_4O_{12}$ and $Pr_2Te_2O_7$. In the former, the Te^{4+} cation is located at the center of a perfect TeO_6 octahedron (Te-O = 2.11 Å) (Siritanon *et al.*, 2011).

The present localization method was applied to 227 oxide structures involving one kind of LP cation (Te^{4+}) in 456 non-equivalent positions. Results are gathered in Table 1 and Figure 4 and Figure 5. The Te-LP distances vary between 0.00 Å and 1.78 Å with an average value of 1.09 Å and a small standard deviation of 0.21 Å. Without considering $Cs_2Te_4O_{12}$ and $Pr_2Te_2O_7$ for which the LP is not stereochemically active, the shortest Te-LP distance (0.48 Å) is obtained in $Rb_4Te_8O_{23}$ and the longest one (1.78 Å) in $Mn_2Te_3O_8$. Concerning the LP radii, they vary between 0.68 Å and 1.49 Å with an average value of 1.11 Å and a small standard deviation of 0.11 Å. The shortest values are found in $Pr_2Te_2O_7$ (0.68 Å), $Cs_2Te_4O_{12}$ (0.71 Å) and $Nb_2Te_3O_{11}$ (0.83 Å), the longest one in $Ga_2Te_3O_9$ (1.56 Å).

At the best of our knowledge, there is only one experiment (Kondratyuk *et al.*, 1987) dealing with the LP localization in TeO_2-based materials. This study was performed on α-TeO_2 single crystal by X-ray diffraction to obtain its precise electronic density map. It revealed a local electronic density maximum, attributed to the lone pair, situated at about 0.6 Å from the core. Later, an *ab initio* study (Suehara *et al.*, 2004*b*) performed on TeO_4H_4 molecule, with geometry close to the TeO_4 disphenoid found in α-TeO_2, also revealed an electronic density maximum at about 0.6 Å from the core. The studies of Galy *et al.* (1975) and Christy & Mills (2013) on oxide crystal structures respectively gave an average Te-LP distance of 1.25 Å for 15 Te^{4+} environments (1.37 Å for α-TeO_2) and 1.15 Å for 40 Te^{4+} environments (0.88 Å for α-TeO_2).

In order to better understand those differences, we performed a complementary analysis using the ELF function. For 33 oxide structures containing 66 non-equivalent Te^{4+} positions, we calculated the Te-LP distances by considering that the local maximum of ELF function near the Te^{4+} core corresponds to the LP position. The calculations were carried out using the Vienna *ab initio* simulation package (VASP) code 4.6 (Kresse & Hafner, 1993, 1994; Kresse & Furthmüller, 1996*a*,*b*) with the generalized gradient approximation PW91 (GGA-PW91) (Perdew *et al.*, 1992, 1993) and projector augmented-wave (PAW) potentials (Blöchl, 1994; Kresse & Joubert, 1999). Results are reported in Table 2 and Figure 7.

The average Te-LP distance of 0.94 Å is in relatively good agreement with that obtained with our localization method on the same structures (1.05 Å). It is interesting to note that the Te-LP distance for α-TeO_2 from the ELF analysis (0.91 Å) is clearly larger than that corresponding to the maximum of electronic density (0.6 Å), and is in better agreement with that calculated with our localization method (1.04 Å). A domain with high ELF values repels neighboring electrons, and thus is indicative of the intensity of the LP steric effect. This certainly explains the better agreement between the results obtained with our method and the ELF analysis and also suggests that the electronic density is not the best measure of the LP steric effect. While the agreement with the ELF analysis is particularly good for average values, one can notice a large dispersion of Te-LP distances obtained with our method. In particular, the method led to distances as large as 1.78 Å (for $Mn_2Te_3O_8$). It is unlikely that the maximum of the LP electron density or electron pair probability be actually shifted to such extreme values from the core. This is supported by the fact that the maximum ELF values are found closer to the core, at distances lower than 1.2 Å. Instead, such large values probably indicate a substantial departure of the LP electron density (and electron pair probability) from a spherical symmetry, retaining the main part of the electron density close to the core. This nevertheless also indicates that the neighboring anions are strongly repelled from the core,

leading to a large empty space along the LP direction. To emphasize this point, we applied our method by fixing the LP radius to a constant value, typical of Te^{4+} cation. We used a value of 1.05 Å, which is both close to the value found for the reference α-TeO_2 compound and to the average radius obtained from the linear trend of §3.1. The obtained results are given in Table 2 and Figure 7. We can observe a clear reduction of the dispersion as well as a closer agreement with the ELF analysis, in particular an identical average Te-LP distance of 0.94 Å. Note that as already seen on Figure 5, this effect clearly depends on the nature of the LP cation. With Tl^+ cation for example, the possibility of creating large empty space is much more limited, as suggested by the corresponding small slope given in the plot of Figure 5. If we now compare those results with data of literature related to tellurite crystal structures, one can notice that the average Te-LP distance obtained by Galy *et al.* (1.25 Å) is larger than the above average values obtained with our method and the ELF analysis (the same is true in the case of α-TeO_2 with a distance of 1.37 Å). This may be due to the fact that their method considers that the LP radius is equal to the average radius of the neighboring anions, which could induce an overestimation of the LP size and in turn an overestimation of the Te-LP distance. Finally, our results are close to those obtained by Christy & Mills (2013).

3.2.2. Non-oxide crystal structures

This part focuses on the Te^{4+} LP in the rare cases of non-oxide compounds in order to analyze the effect of the kind of anion. The method was applied to 47 structures containing only one LP cation type (Te^{4+}) in 59 non-equivalent positions and one anion type (X) among Br^-, Cl^-, F^-, I^-, S^{2-} and Se^{2-}. The Te-LP distances and Te^{4+} LP radii are presented in Table 3 and Figure 8; those related to O^{2-} are included for comparison. Overall, the values tend to be smaller in environments implying larger and less charged anions. The smallest average distances and radii are indeed observed with Br^- and I^- (Te-LP distances of 0.32 Å and 0.35 Å respectively; Te^{4+} LP radii of 0.77 Å in both cases). For each anion type, the LP radius increases linearly

with the Te-LP distance as observed in oxide structures. These results can still be explained with the bond valence concept. With small anions, the Te^{4+} valence is reached with a low number of neighboring anions due to short Te-X bonds, implying that anions of the second-coordination sphere are far from the core. Consequently, the lone pair can displace away from the core. With larger anions, the Te-X primary bonds are longer so the cation valence can only be reached by increasing the coordination number, inducing a more symmetric environment, a smaller Te-LP distance and a smaller LP radius.

In most cases, Te^{4+} cation has a stereoactive lone pair, the only exceptions being observed within perfect or quasi-perfect octahedra. Besides $Cs_2Te_4O_{12}$ and $Pr_2Te_2O_7$ (r_{LP} = 0.71 Å and 0.68 Å respectively), the LP radius is equal to 0.74 Å in Cs_2TeBr_6 and 0.72 Å in K_2TeBr_6, Rb_2TeBr_6, K_2TeI_6 and Rb_2TeI_6. A Te^{4+} cation whose lone pair is inactive can thus be modeled by a hard sphere of 0.72 Å in radius whatever the surrounding anionic species.

4. Conclusion

A systematic study was performed on oxide structures and on Te^{4+}-containing non-oxide structures in order to improve the local structural description of compounds containing cations of the p-block elements carrying a lone electron pair.

We developed a simple method based on pure geometrical concepts to localize lone pairs and model their steric effect regardless the LP cation types and their environment.

This method was applied to 1185 structures containing one LP cation type in 2439 non-equivalent positions and one anion type, using the 'LPLoc' program (Hamani & Masson, 2019).

In the periodic table, from bottom left to top right, the overall trends for oxide crystal structures are that the lone pair moves away from its core (with respect to the cation core and LP sizes) and the LP size decreases (r_{LP} = 1.52 Å for Tl^{+} and 0.40 Å for Cl^{5+}). For one cationic species, the evolution of the LP radius reveals a linear increase more or less

pronounced with the M*-LP distance: the Tl^{+} cation retains a lone pair of quasi-constant size whatever the oxide structure, whereas in the case of Cl^{5+}, the LP size distinctly increases with the Cl-LP distance.

The influence of different anions for one LP cation type was also studied in the case of Te^{4+}. For each anion type, the same trend as in oxide structures is observed, namely a linear increase of the LP radius with the Te-LP distance. Overall, the smallest Te-LP distances and LP radii are found for anions of large size and small charge (bottom right of the periodic table).

The universal character of the proposed method, applied to crystalline compounds in this study, could be transposed to amorphous compounds in order to improve their structural description at atomic scale.

Figures

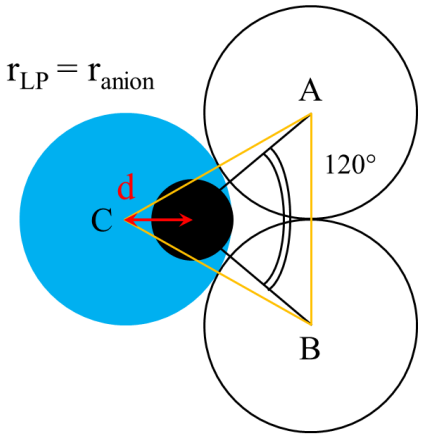

Figure 1. Illustration of the principle of the LP localization method developed by Galy et al. (1975) in the case of a plane environment. The M core is in black, LP in blue and anions in open circles. The M*-LP distance d is calculated so that AB = AC = BC. (Figure inspired from Galy et al., 1975)*

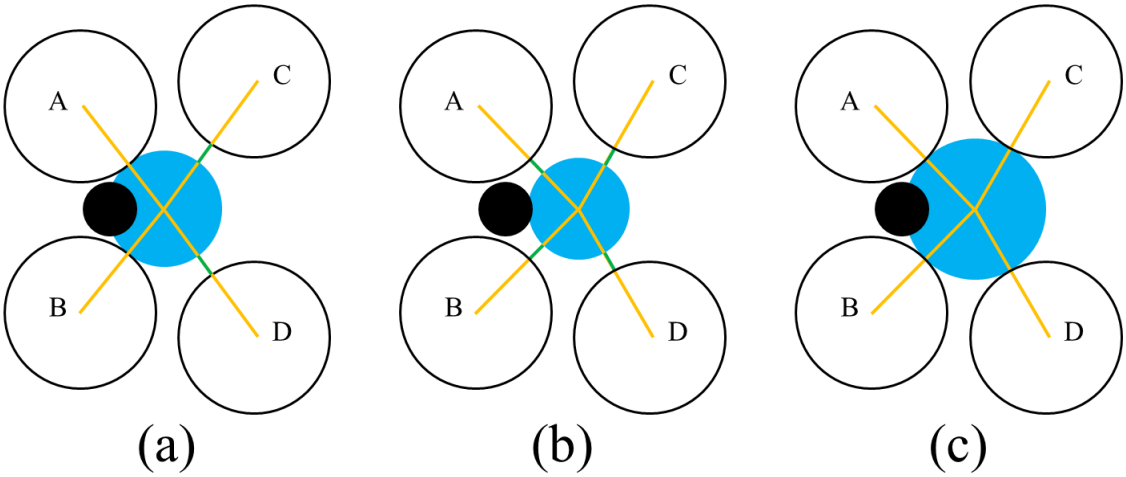

Figure 2. Illustration of the principle of the present LP localization method. The M core are in black, LP in blue and anions in open circles: (a) the LP is too close to anions A and B, (b) the LP is at the optimum position but its radius is too small, (c) both position and radius of the LP are optimum and minimize the sum of distances (SoD).*

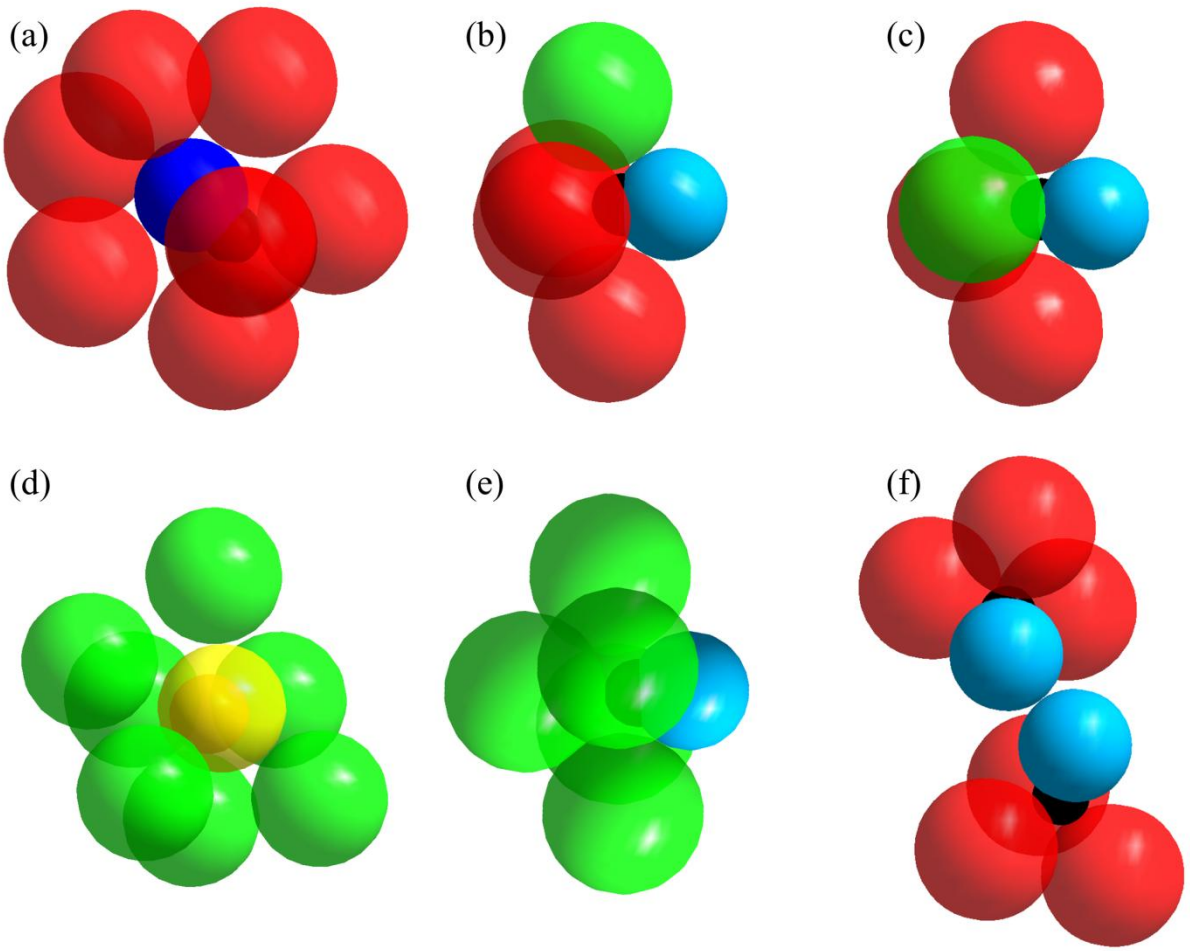

Figure 3. Graphical representations (space-filling model) of the results obtained by applying the present method to LP cations in specific compounds: (a) Te^{4+} in α-TeO_2 (ICSD #62898), (b and c) Te^{4+} (2 different sites) in $Te_2O_3F_2$ (#82162), (d and e) Pb^{2+} and Te^{4+} in $PbTeF_6$ (#81865) and (f) Te^{4+} in α-$CdTeO_3$ (#60067). Te^{4+} cores are in black, Te^{4+} LPs in blue, Pb^{2+} core in orange, Pb^{2+} LP in yellow, O^{2-} anions in red and F^- anions in green. Radii of the Te^{4+} cores, Pb^{2+} core, O^{2-} and F^- anions are 0.56 Å, 0.775 Å, 1.40 Å and 1.33 Å respectively.

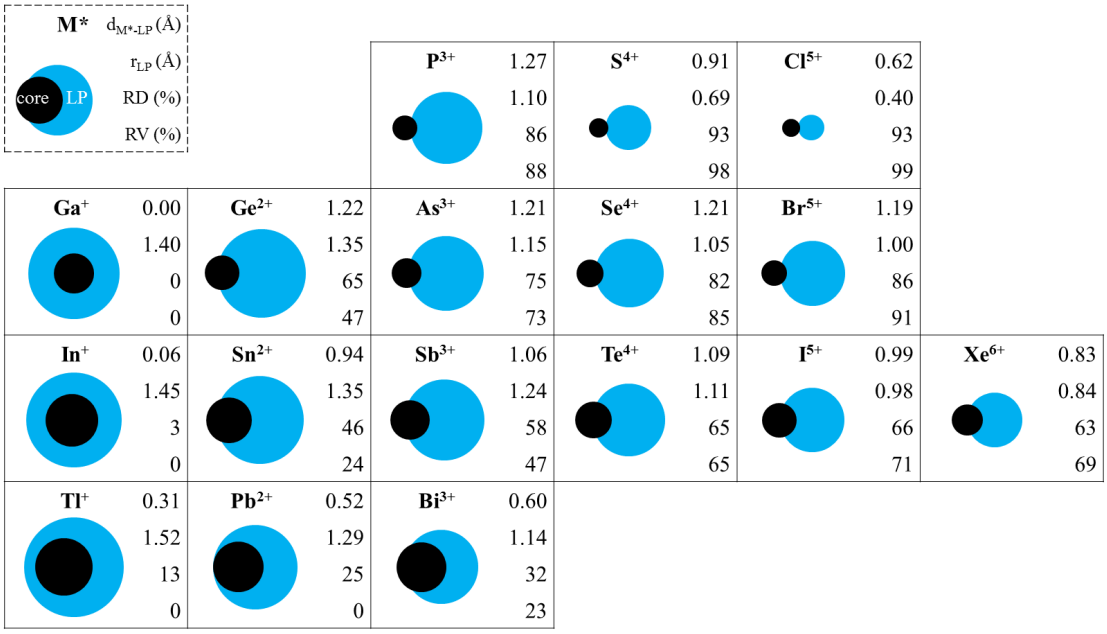

Figure 4. Schematic representations of the LP size and displacement (from the core) with respect to the position of the cation M in the periodic table. The cores are in black and LPs in blue. The average M*-LP distances, LP radii, relative displacements and relative volumes (see text) given for each cation were obtained from 2380 non-equivalent M* positions in 1138 oxide crystal structures.*

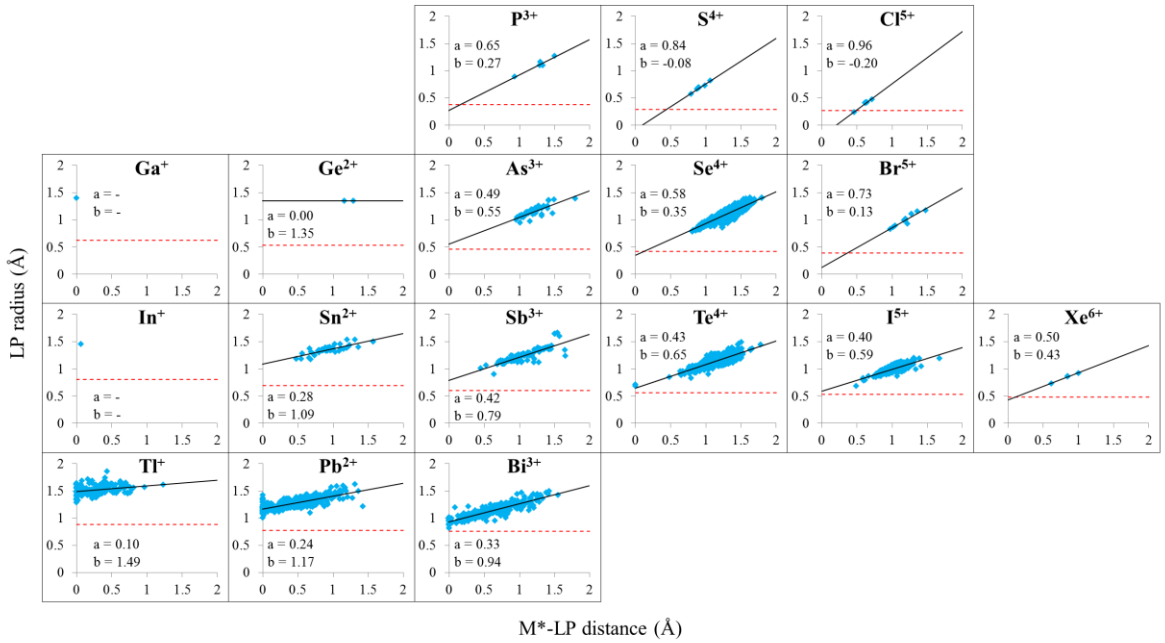

Figure 5. Variation of the LP radius as a function of the M-LP distance for cations of the p-block elements based on 2380 non-equivalent M* positions in 1138 oxide crystal structures. The dashed red line indicates the core radius value, a and b are the slope and the intercept at the origin of the linear regression (black line) respectively.*

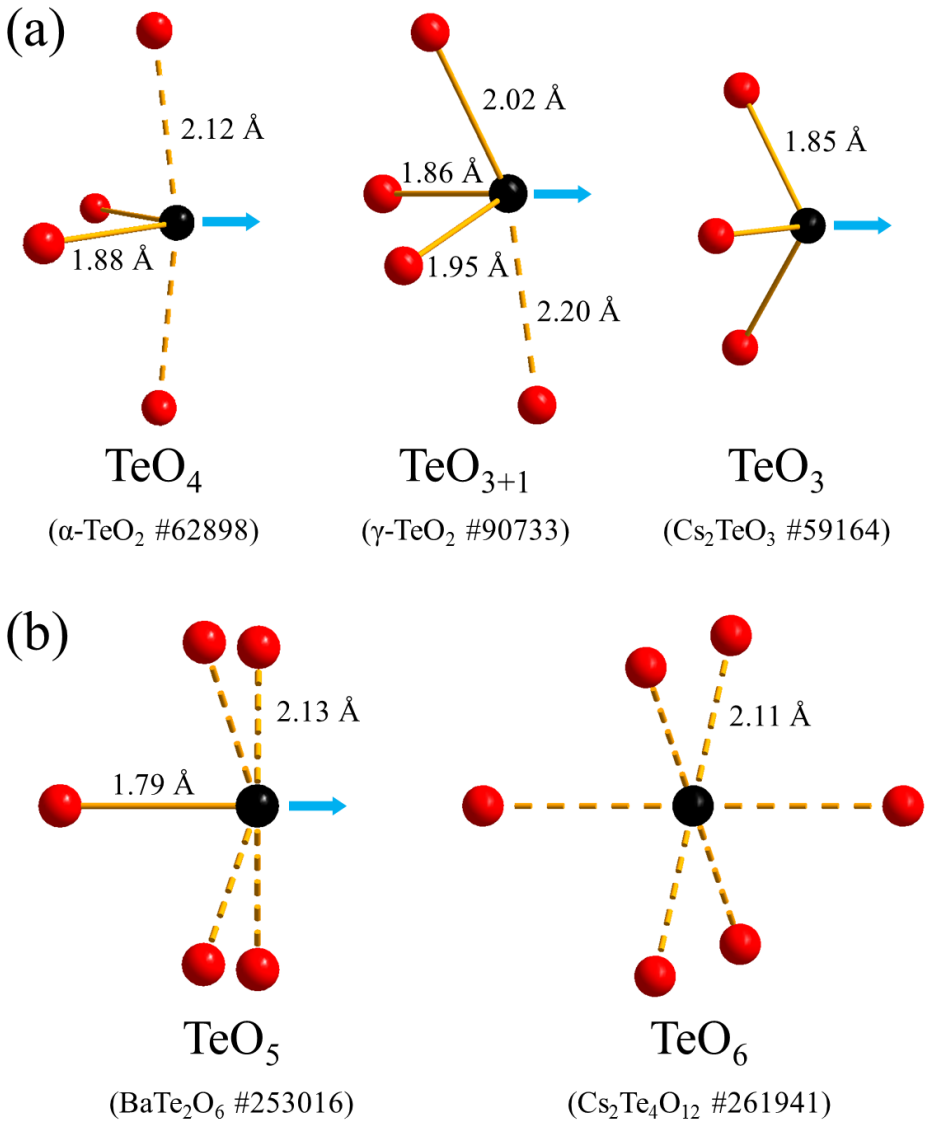

Figure 6. Local environments of Te^{4+} cations found in TeO_2-based crystal structures: (a) usual environments, (b) atypical environments. Te^{4+} cores are in black, O^{2-} anions in red, blue arrows represent Te^{4+} LPs and longest Te-O bonds are drawn with dashed lines. Typical compound illustrative of each environment is given in brackets as well as the collection code of its ICSD entry.

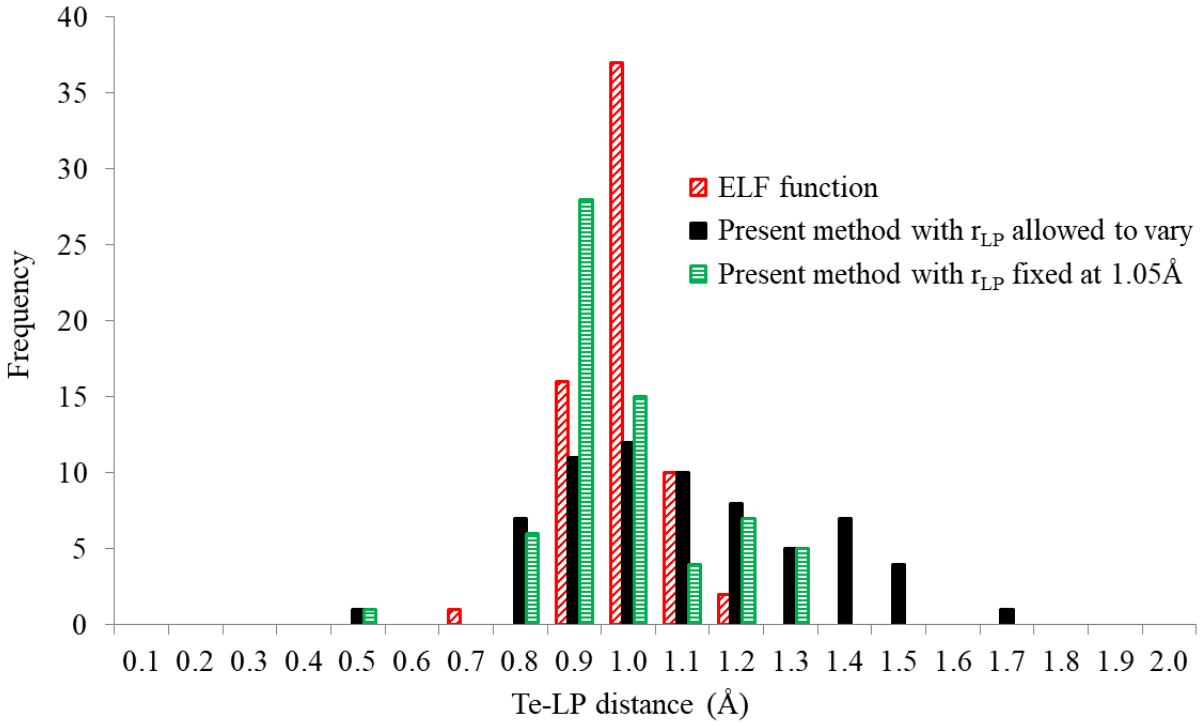

Figure 7. Comparison of the distributions of the Te-LP distances obtained with the present method and using the ELF function, based on 66 non-equivalent Te^{4+} positions in 33 oxide crystal structures. The bin width is 0.1 Å.

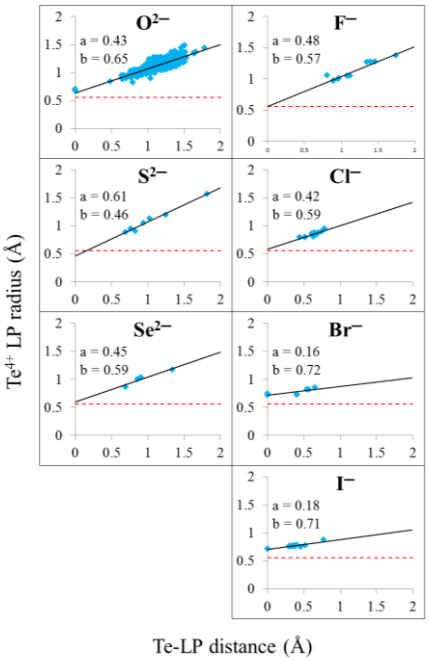

Figure 8. Comparison of the variation of the Te^{4+} LP radius as a function of the Te-LP distance for different kinds of anions. The dashed red line indicates the core radius value (0.56 Å), a and b are the slope and the intercept at the origin of the linear regression (black line) respectively.

Tables

M*	Number of structures	Number of non-equivalent positions	Core radius (Å)	$d_{M^*\text{-}LP}$ (Å)				r_{LP} (Å)				Average relative displacement (RD, %)	Average relative volume (RV, %)
				Average	Standard deviation	Min.	Max.	Average	Standard deviation	Min.	Max.		
As^{3+}	25	43	0.46	1.21	0.17	0.96	1.80	1.15	0.10	0.94	1.39	75	73
Bi^{3+}	179	365	0.76	0.60	0.31	0.00	1.55	1.14	0.12	0.82	1.50	32	23
Br^{5+}	9	10	0.39	1.19	0.16	0.97	1.48	1.00	0.12	0.83	1.17	86	91
Cl^{5+}	7	7	0.27	0.62	0.07	0.46	0.71	0.40	0.07	0.24	0.47	93	99
Ga^{+}	1	1	0.62	0.00	-	0.00	0.00	1.40	-	1.40	1.40	0	0
Ge^{2+}	1	2	0.53	1.22	0.09	1.16	1.28	1.35	0.00	1.35	1.35	65	47
I^{5+}	94	278	0.53	0.99	0.15	0.49	1.67	0.98	0.08	0.68	1.20	66	71
In^{+}	1	1	0.80	0.06	-	0.06	0.06	1.45	-	1.45	1.45	3	0
P^{3+}	3	5	0.38	1.27	0.21	0.94	1.50	1.10	0.14	0.89	1.27	86	88
Pb^{2+}	207	447	0.775	0.52	0.30	0.00	1.42	1.29	0.09	1.01	1.62	25	0
S^{4+}	7	9	0.29	0.91	0.08	0.79	1.07	0.69	0.07	0.57	0.82	93	98
Sb^{3+}	60	120	0.60	1.06	0.25	0.45	1.65	1.24	0.12	0.90	1.66	58	47
Se^{4+}	211	439	0.42	1.21	0.18	0.80	1.79	1.05	0.12	0.79	1.41	82	85
Sn^{2+}	25	48	0.69	0.94	0.23	0.48	1.57	1.35	0.08	1.17	1.53	46	24
Te^{4+}	227	456	0.56	1.09	0.21	0.00	1.78	1.11	0.11	0.68	1.49	65	65
Tl^{+}	78	145	0.885	0.31	0.24	0.00	1.24	1.52	0.09	1.29	1.86	13	0
Xe^{6+}	3	4	0.48	0.83	0.16	0.61	1.00	0.84	0.08	0.73	0.92	63	69

Table 1. Average M-LP distances, LP radii, relative displacements and relative volumes (see text) obtained from 2380 non-equivalent M* positions in 1138 oxide crystal structures.*

Method	$d_{Te\text{-}LP}$ (Å)			
	Average	Standard deviation	Min.	Max.
ELF function	0.94	0.08	0.69	1.15
Present method with r_{LP} allowed to vary	1.05	0.22	0.48	1.66
Present method with r_{LP} fixed at 1.05 Å	0.94	0.15	0.42	1.24

Table 2. Comparison of the average Te-LP distances obtained with the present method and using the ELF function, based on 66 non-equivalent Te^{4+} positions in 33 oxide crystal structures

X	Number of structures	Number of non-equivalent positions	Anion radius (Å)	$d_{Te\text{-}LP}$ (Å)				r_{LP} (Å)			
				Average	Standard deviation	Min.	Max.	Average	Standard deviation	Min.	Max.
Br^{-}	7	8	1.96	0.32	0.28	0.00	0.65	0.77	0.05	0.72	0.85
Cl^{-}	14	15	1.81	0.62	0.09	0.44	0.78	0.85	0.04	0.80	0.95
F^{-}	9	11	1.33	1.15	0.29	0.81	1.74	1.12	0.15	0.97	1.38
I^{-}	7	14	2.20	0.35	0.19	0.00	0.77	0.77	0.04	0.72	0.88
O^{2-}	227	456	1.40	1.09	0.21	0.00	1.78	1.11	0.11	0.68	1.49
S^{2-}	6	7	1.84	1.05	0.39	0.70	1.82	1.10	0.24	0.89	1.57
Se^{2-}	4	4	1.98	0.95	0.27	0.69	1.34	1.02	0.13	0.86	1.17

Table 3. Comparison of the average Te-LP distances and Te^{4+} LP radii obtained for seven different kinds of anions (X).

References

Allmann, P. D. R. (1975). *Monatshefte Für Chem. Chem. Mon.* **106**, 779–793.

Andersson, S. & Åström, A. (1972). *Natl. Bur. Stand.* **SP364. Solid State Chemistry. Proceedings of the 5th Materials Research Symposium, 3–14.**

Balić Žunić, T. & Makovicky, E. (1996). *Acta Crystallogr. B.* **52**, 78–81.

Becke, A. D. & Edgecombe, K. E. (1990). *J. Chem. Phys.* **92**, 5397–5403.

Becker, C. R., Tagg, S. L., Huffman, J. C. & Zwanziger, J. W. (1997). *Inorg. Chem.* **36**, 5559–5564.

Berski, S., Gajewski, G. & Latajka, Z. (2007). *J. Mol. Struct.* **844–845**, 278–285.

Blöchl, P. E. (1994). *Phys. Rev. B.* **50**, 17953–17979.

Brown, I. D. (1978). *Chem. Soc. Rev.* **7**, 359–376.

Brown, I. D. (2011). *J. Phys. Chem. A.* **115**, 12638–12645.

Brown, I. D. (2016). The Chemical Bond in Inorganic Chemistry: The Bond Valence Model Oxford: Oxford University Press.

Chesnut, D. B. (2000). *J. Phys. Chem. A.* **104**, 11644–11650.

Christy, A. G. & Mills, S. J. (2013). *Acta Crystallogr. Sect. B Struct. Sci. Cryst. Eng. Mater.* **69**, 446–456.

Christy, A. G., Mills, S. J. & Kampf, A. R. (2016). *Mineral. Mag.* **80**, 415–545.

Fargin, E., Berthereau, A., Cardinal, T., Le Flem, G., Ducasse, L., Canioni, L., Segonds, P., Sarger, L. & Ducasse, A. (1996). *J. Non-Cryst. Solids*. **203**, 96–101.

Galy, J., Couégnat, G., Vila, E. & Matar, S. F. (2017). *Comptes Rendus Chim.* **20**, 446–459.

Galy, J. & Matar, S. F. (2016). *Prog. Solid State Chem.* **44**, 35–58.

Galy, J. & Matar, S. F. (2018). *Solid State Sci.* **82**, 44–51.

Galy, J. & Matar, S. F. (2019). *Prog. Solid State Chem.* **56**, 100252.

Galy, J., Meunier, G., Andersson, S. & Åström, A. (1975). *J. Solid State Chem.* **13**, 142–159.

Galy, J. & Vignoles, G. L. (2020). *Solid State Sci.* **100**, 106068.

Gillespie, R. J. & Nyholm, R. S. (1957). *Q. Rev. Chem. Soc.* **11**, 339–380.

Hall, S. R., Allen, F. H. & Brown, I. D. (1991). *Acta Crystallogr. A.* **47**, 655–685.

Hamani, D. (2010). Cristallochimie de matériaux à base de dioxyde de tellure : vers un modèle structural pour l'étude des composés vitreux. thesis. Université de Limoges.

Hamani, D. & Masson, O. (2019). LPLoc program. IRCER - UMR CNRS 7315, Université de Limoges, France. The software is freely available on request from the authors.

Jeansannetas, B., Blanchandin, S., Thomas, P., Marchet, P., Champarnaud-Mesjard, J. C., Merle-Méjean, T., Frit, B., Nazabal, V., Fargin, E., Le Flem, G., Martin, M. O., Bousquet, B., Canioni, L., Le Boiteux, S., Segonds, P. & Sarger, L. (1999). *J. Solid State Chem.* **146**, 329–335.

Kondratyuk, I. P., Muradyan, L. A., Pisarevskii, Yu. V. & Simonov, V. I. (1987). *Kristallografiya*. **32**, 609–617.

Kresse, G. & Furthmüller, J. (1996*a*). *Comput. Mater. Sci.* **6**, 15–50.

Kresse, G. & Furthmüller, J. (1996*b*). *Phys. Rev. B.* **54**, 11169–11186.

Kresse, G. & Hafner, J. (1993). *Phys. Rev. B.* **47**, 558–561.

Kresse, G. & Hafner, J. (1994). *Phys. Rev. B.* **49**, 14251–14269.

Kresse, G. & Joubert, D. (1999). *Phys. Rev. B.* **59**, 1758–1775.

Matar, S. F. & Galy, J. (2015). *Prog. Solid State Chem.* **43**, 82–97.

Mirgorodsky, A. P., Merle-Méjean, T., Thomas, P., Champarnaud-Mesjard, J.-C. & Frit, B. (2002). *J. Phys. Chem. Solids*. **63**, 545–554.

Perdew, J. P., Chevary, J. A., Vosko, S. H., Jackson, K. A., Pederson, M. R., Singh, D. J. & Fiolhais, C. (1992). *Phys. Rev. B.* **46**, 6671–6687.

Perdew, J. P., Chevary, J. A., Vosko, S. H., Jackson, K. A., Pederson, M. R., Singh, D. J. & Fiolhais, C. (1993). *Phys. Rev. B.* **48**, 4978–4978.

Rahm, M. & Christe, Karl. O. (2013). *ChemPhysChem*. **14**, 3714–3725.

Roginskii, E. M., Kuznetsov, V. G., Smirnov, M. B., Noguera, O., Duclère, J.-R., Colas, M., Masson, O. & Thomas, P. (2017). *J. Phys. Chem. C*. **121**, 12365–12374.

Seshadri, R. (2001). *J. Chem. Sci.* **113**, 487–496.

Shannon, R. D. (1976). *Acta Crystallogr.* **A32**, 751–767.

Siritanon, T., Li, J., Stalick, J. K., Macaluso, R. T., Sleight, A. W. & Subramanian, M. A. (2011). *Inorg. Chem.* **50**, 8494–8501.

Soulis, M., Merle-Méjean, T., Mirgorodsky, A. P., Masson, O., Orhan, E., Thomas, P. & Smirnov, M. B. (2008). *J. Non-Cryst. Solids*. **354**, 199–202.

Suehara, S., Thomas, P., Mirgorodsky, A., Merle-Méjean, T., Champarnaud-Mesjard, J. C., Aizawa, T., Hishita, S., Todoroki, S., Konishi, T. & Inoue, S. (2004*a*). *J. Non-Cryst. Solids*. **345–346**, 730–733.

Suehara, S., Thomas, P., Mirgorodsky, A. P., Merle-Méjean, T., Champarnaud-Mesjard, J. C., Aizawa, T., Hishita, S., Todoroki, S., Konishi, T. & Inoue, S. (2004*b*). *Phys. Rev. B.* **70**, 205121.

Tagg, S. L., Huffman, J. C. & Zwanziger, J. W. (1994). *Chem. Mater.* **6**, 1884–1889.

Urusov, V. S. (2003). *Z. Für Krist.* **218**, 709–719.

Verbaere, A., Marchand, R. & Tournoux, M. (1978). *J. Solid State Chem.* **23**, 383–390.

Wallez, G. (1999). HYBRIDE: a program for the research of lone pairs positions in crystalline solids.

(*a*). Crystallographic Information File project of the International Union of Crystallography.

(*b*). Inorganic Crystal Structure Database, Fachinformationszentrum Karlsruhe.